University of Groningen

Efficient spin injection into graphene through trilayer hBN tunnel barriers

Leutenantsmeyer, Johannes Christian; Ingla-Aynes, Josep; Gurram, Mallikarjuna; van Wees, Bart J.

IMPORTANT NOTE: You are advised to consult the publisher's version (publisher's PDF) if you wish to cite from it. Please check the document version below.

Document Version
Publisher's PDF, also known as Version of record

Publication date:
2018

Link to publication in University of Groningen/UMCG research database

Efficient spin injection into graphene through trilayer hBN tunnel barriers

Johannes Christian Leutenantsmeyer, Josep Ingla-Aynés, Mallikarjuna Gurram, and Bart J. van Wees

---

Efficient spin injection into graphene through trilayer hBN tunnel barriers

Johannes Christian Leutenantsmeyer,[a),b)] Josep Ingla-Aynés,[a)] Mallikarjuna Gurram, and Bart J. van Wees

Physics of Nanodevices, Zernike Institute for Advanced Materials University of Groningen, 9747 AG Groningen, The Netherlands

We characterize the spin injection into bilayer graphene fully encapsulated in hexagonal boron nitride (hBN) including a trilayer (3L) hexagonal boron nitride (hBN) tunnel barrier. As a function of the DC bias, the differential spin injection polarization is found to rise to -60% at -250 mV DC bias voltage. We measure a DC spin polarization of $\sim 50\%$, 30% higher compared to 2L-hBN. The large polarization is confirmed by local, two terminal spin transport measurements up to room temperature. We observe comparable differential spin injection efficiencies from Co/2L-hBN and Co/3L-hBN into graphene and conclude that the possible exchange interaction between cobalt and graphene is likely not the origin of the bias dependence. Furthermore, our results show that local gating arising from the applied DC bias is not responsible for the DC bias dependence. Carrier density dependent measurements of the spin injection efficiency are discussed, where we find no significant modulation of the differential spin injection polarization. We also address the bias dependence of the injection of in-plane and out-of-plane spins and conclude that the spin injection polarization is isotropic and does not depend on the applied bias. *Published by AIP Publishing.*
https://doi.org/10.1063/1.5050874

I. INTRODUCTION

Graphene is an ideal material for long distance spin transport due to its low intrinsic spin-orbit coupling and outstanding electronic quality.[1–5] Experimental results have shown that long spin relaxation lengths require the protection of the graphene channel from contamination.[4–7] The most effective way to achieve this is the encapsulation of graphene with hexagonal boron nitride (hBN), which substantially improved the spin transport properties.[5–11] Besides the cleanliness of the channel, the efficient injection and detection of spins into graphene is an essential requirement to fabricate high performance devices. To circumvent the conductivity mismatch problem,[12] a tunnel barrier is employed to enhance the spin injection polarization.[13] Commonly used AlO_2 and TiO_2 tunnel barriers have been extensively used in graphene spintronics but yield typically spin polarizations below 10%.[14] The use of crystalline MgO,[15–17] hBN,[18–22] amorphous carbon,[23] or SrO[24] as a tunnel barrier has led to significant enhancements. In particular, the use of a 2L-hBN flake for spin injection gives rise to bias dependent differential spin injection polarizations p_{in} up to $p_{in} = 70\%$, which is defined as the injected AC spin current i_s divided by the AC charge current i_{AC}. Furthermore, 2L-hBN provides contact resistances in the range of $10 \, k\Omega$, which can be close to the spin resistance of high quality graphene and affect spin transport.[21] 3L-hBN tunnel barriers promise higher contact resistances, leaving the spin transport in 3L-hBN/graphene unaffected.[20,25]

While the underlying mechanism for the DC bias dependent spin injection is still unclear, *ab initio* calculations of

cobalt separated from graphene by hBN show that in the optimal case Co can induce an exchange interaction of 10 meV even through 2L-hBN into graphene.[26] Therefore, a comparison between hBN tunnel barriers of different thicknesses can give insight on the proximity effects between graphene and cobalt.

Here, we show that 3L-hBN tunnel barriers increase the differential spin injection polarization into bilayer graphene (BLG) from a zero bias value of $p = 20\%$ up to values above $p_{in} = -60\%$ at -250 mV DC bias voltage. The DC spin injection polarization P, which is defined as the DC spin current I_s divided by the DC charge current I_{DC}, increases up to $P = 50\%$, at a DC bias current of $-2 \, \mu A$. This is a substantial advantage over 2L-hBN, which shows $P \sim 35\%$. The large DC spin polarization allows us to measure spin signals in a DC two-terminal spin valve geometry up to room temperature. We show that the differential spin injection polarization is, contrary to Ringer *et al.*,[27] independent of the carrier density. The rotation of the magnetization of the electrodes out-of-plane under a perpendicular magnetic field $B_\perp$ allows us to study the bias dependence of the spin injection polarization of out-of-plane spins (p_z). We compare p_z with the in-plane polarization p_y and conclude that $p_z/p_y \sim 1$, independently of the applied DC bias.

II. SAMPLE PREPARATION AND CONTACT CHARACTERIZATION

The 3L-hBN/bilayer graphene (BLG)/bottom-hBN stack is fabricated using the scotch tape technique to exfoliate hBN from hBN powder (HQ Graphene) and graphene from HOPG (ZYB grade, HQ Graphene). BLG is encapsulated between a 5 nm thick bottom hBN and a 1.2 nm thick 3L-hBN flake, which acts as a tunnel barrier. The materials are stacked

using a polycarbonate based dry transfer technique[28] and deposited on a silicon oxide substrate with 90 nm oxide thickness, which is used to tune the carrier concentration in the graphene channel. The transfer polymer is removed in chloroform, and the sample is annealed for 1 h in Ar/H_2. PMMA is spun on the sample, and contacts are exposed using e-beam lithography. The sample is developed in a 1:3 mixture of MIBK:IPA, and 65 nm Co and 5 nm Al as capping layer are deposited. The PMMA mask is removed in warm acetone. The sample is bonded on a chip carrier and loaded into a cryostat where the sample space is evacuated below 10^{-6} mbar. The geometry of the resulting device is shown in Fig. 1(a). This device has been used to study the spin lifetime anisotropy in BLG and has a mobility of 12 000 cm^2/Vs.[29] Unless noted, all measurements are carried out at $T = 75$ K to improve the signal to noise ratio.

The atomic force microscopy image of the stack before the contact deposition is shown in Fig. 1(b). The contact resistances are characterized by measuring the bias dependence in the three terminal geometry, $R_c = V_{3T}/I_{DC}$, and shown in Fig. 1(c) as a function of the voltage applied across the 3L-hBN tunnel barrier (V_{3T}). The bias dependent contact resistances are normalized to the contact area and plotted as a function of the DC current I_{DC} applied to the hBN barrier in Fig. 1(d). To determine the spin transport properties of our device, we use the standard non-local geometry,[30–32] the circuit is shown in Fig. 1(a). An AC charge current i_{AC} is applied together with I_{DC} between the injector and the left reference contact, which does not have any tunnel barrier and therefore does not inject spins efficiently. Because of the spin polarization of the cobalt/hBN contacts, the injected charge current is spin polarized and

induces a spin accumulation into the channel. The spins diffuse in the BLG channel and are detected by a second cobalt/hBN contact in the non-local geometry.

III. SPIN TRANSPORT AT DIFFERENT DC BIAS CURRENTS

The different coercive fields of the cobalt contacts allow the separate switching of individual electrodes with an in-plane magnetic field $B_{\parallel}$ and the measurement of the non-local resistance ($R_{NL} = v_{NL}/i_{AC}$) in different magnetic configurations. The non-local spin valve is shown in Fig. 2(a) for different DC bias currents. The abrupt signal changes are caused by the switching of the contact magnetization, and the magnetization configurations are indicated with arrows. The spin signal R_{NL} is determined by the difference between parallel [$R_{NL}(\uparrow\uparrow) = R_{NL}(\downarrow\downarrow)$] and antiparallel [$R_{NL}(\uparrow\downarrow) = R_{NL}(\downarrow\uparrow)$] configurations.

The most accurate way to characterize the spin transport properties of the channel is using spin precession, where the magnetic field is applied perpendicular to the BLG plane ($B_{\perp}$), causing spins to precess in the x-y-plane. By fitting R_{NL} to the Bloch spin diffusion equations, we extract the spin lifetime (τ_s), spin diffusion coefficient (D_s), and the average polarization of both electrodes (p_y). The data are shown for different DC bias currents in Fig. 2(b), and the fitting curves are shown as solid lines. Note that the spin transport parameters in Table I are within the experimental uncertainty for all I_{DC} values. Therefore, we average τ_s, D_s, and the spin relaxation length (λ) over all four values and obtain $\tau_s = (1.9 \pm 0.2)$ ns, $D_s = (183 \pm 17)$ cm^2/s, and $\lambda = \sqrt{D_s\tau_{\parallel}} = (5.8 \pm 0.6)$ µm. These parameters are comparable to the ones reported in Ref. 25. We conclude that the change in contact resistance with I_{DC} does not affect the spin transport for values above 100 kΩ. This is caused by
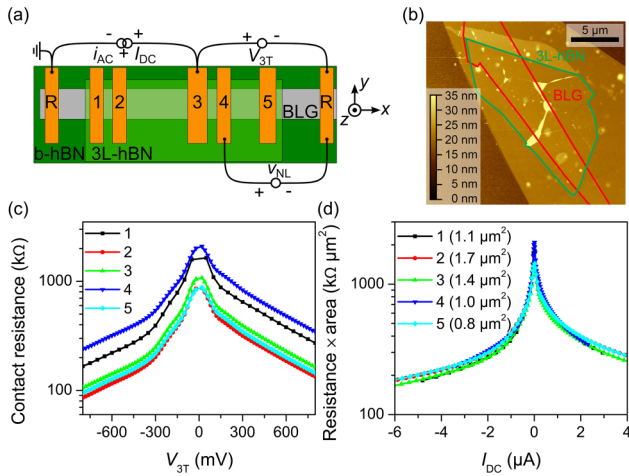

FIG. 1. (a) Schematic device geometry. A BLG flake is encapsulated between a 5 nm thick hBN (b-hBN) and a 1.2 nm 3L-hBN flake, used as a tunnel barrier for spin injection. Note that the outer reference contacts (R) do not have an hBN tunnel barrier. The different measurement geometries are sketched. We apply a DC current I_{DC} and additionally an AC measurement current i_{AC} to the injector contact. We measure the DC voltage V_{3T} in a three-terminal geometry and calculate the contact resistance $R_c = V_{3T}/I_{DC}$. The AC non-local voltage (v_{NL}) is used to calculate the non-local resistance $R_{NL} = v_{NL}/i_{AC}$. (b) Atomic force microscopy image of the hBN/BLG/3L-hBN heterostructure before the contact deposition. (c) Contact resistance measurements for different voltages applied across the hBN tunnel barrier (V_{3T}). (d) The calculated resistance-area products ($R_c \times A$) range between 180 kΩµm^2 and 2 MΩµm^2, depending on the applied DC bias current I_{DC}.

FIG. 2. Characterization of the spin transport in the fully hBN encapsulated BLG device at different DC bias currents using Contact 1 as injector and Contact 5 as detector. Both electrodes are separated by $L = 10$ µm. (a) Non-local resistance (R_{NL}) measured in an in-plane magnetic field $B_{\parallel}$ where the magnetization of the injector and detector contacts is switched between parallel and antiparallel alignment. (b) Spin precession measurement in an out-of-plane magnetic field $B_{\perp}$. The fitting using the Bloch equations yields the spin transport parameters shown in Table I. Note that non-local background resistances smaller than 35 Ω have been subtracted from the data to compare the influence of the different DC bias.

TABLE I. Spin transport parameters extracted from the data shown in Fig. 2(b). The values obtained from averaging over the different I_{DC} are $D_s = (183 \pm 17)\,\mathrm{cm^2/s}$, $\tau_s = (1.9 \pm 0.2)\,\mathrm{ns}$, and $\lambda = (5.8 \pm 0.6)\,\mu\mathrm{m}$.

I_{DC} (μA)	$R_c \times A$ (k$\Omega\mu$m^2)	D_s (cm^2/s)	τ_s (ns)	λ (μm)
-2	280	208 ± 25	2.1 ± 0.2	6.4 ± 1.6
-0.6	760	177 ± 21	1.7 ± 0.2	5.5 ± 1.2
0	2100	171 ± 24	1.7 ± 0.2	5.4 ± 1.5
$+2$	380	177 ± 24	2.0 ± 0.2	5.8 ± 1.5

the fact that the contact resistance remains clearly above the spin resistance of the channel $R_s = R_{sq}\lambda/w \sim 1.8\,\mathrm{k\Omega}$, where R_{sq} is the graphene square resistance and w the graphene width.[33]

Note that the spin resistance of graphene can exceed $10\,\mathrm{k\Omega}$ in high quality devices. This is close to the contact resistance of biased 2L-hBN tunnel barriers, which typically range, depending on I_{DC}, between $5\,\mathrm{k\Omega}$ and $30\,\mathrm{k\Omega}$.[34] Furthermore, the extended data sets discussed in the supplementary material and our analysis in Ref. 29 confirm that contact-induced spin back flow is not limiting spin transport for contact resistances above $100\,\mathrm{k\Omega}$.

IV. DC BIAS DEPENDENCE OF THE DIFFERENTIAL SPIN INJECTION EFFICIENCY

In Fig. 3(a), we show the non-local spin valve signal $\Delta R_{NL} = R_{NL}(\uparrow\uparrow) - R_{NL}(\uparrow\downarrow)$. For a comparison with 2L-hBN tunnel barriers, we calculate V_{3T}, the voltage applied to the tunnel barrier, by using the current-voltage characteristics of each contact. To resolve small features in the bias dependence, we source currents as low as $i_{AC} = 50\,\mathrm{nA}$. As observed for 2L-hBN barriers,[21,34] ΔR_{NL} changes sign at $V_{3T} \sim -100\,\mathrm{mV}$, which we also observe with a 3L-hBN barrier. Our data also show additional features: Firstly, $|\Delta R_{NL}|$ shows a maximum at $V_{3T} \sim -250\,\mathrm{mV}$ and decreases again for $V_{3T} < -250\,\mathrm{mV}$. In contrast, we observe a

continuous increase for $V_{3T} > +300\,\mathrm{mV}$. Secondly, we observe a peak at zero V_{3T}, indicating that the polarization of Co/3L-hBN at zero DC bias is higher than in Co/2L-hBN. Note that 2L-hBN devices in Ref. 34 show also these small features around zero DC bias [Fig. 4(b)].

To calculate the polarization of the Co/hBN interface from ΔR_{NL}, we use

$$\Delta R_{NL} = \frac{p_{in}\,p_{det}\,R_{sq}\lambda}{w}e^{-d/\lambda}, \tag{1}$$

where p_{in} and p_{det} are the differential injector and detector spin polarizations and d is the separation between injector and detector. An overview of all extracted spin transport parameters is shown in the supplementary material. Following this procedure for $I_{DC} = 0$ at different configurations, we obtain the unbiased spin polarizations of all contacts, $p_1 = 24\%$, $p_2 = 23\%$, $p_3 = 30\%$, $p_4 = 36\%$, and $p_5 = 38\%$. Since p_{det} does not depend on the DC bias, which is applied to the injector only, we can calculate the bias dependence of p_{in} [Fig. 3(b)]. The absolute sign of p cannot be determined from spin transport measurements,[21] and we define p to be positive for $I_{DC} = 0$.

Note that the slope observed in Fig. 3(b) is in qualitative agreement with the *ab initio* calculations by Piquemal-Banci *et al.*[35] for chemisorbed cobalt on hBN, suggesting that the observed DC bias dependence arises from the Co/hBN interface and not from proximity coupling between cobalt and graphene.

We conclude that $p_{in}(I_{DC})$ can reach values comparable to 2L-hBN tunnel barriers. Moreover, the comparison between different carrier concentrations shows that the spin injection polarization does not depend on the carrier density, even at the charge neutrality point. This also indicates that local spin drift in the barrier arising from pinholes is not responsible for the bias dependence. The drift velocity is inversely proportional to the carrier density, and therefore the effect of spin drift is the largest near the neutrality point.[4] Furthermore, if charge carrier drift in the channel
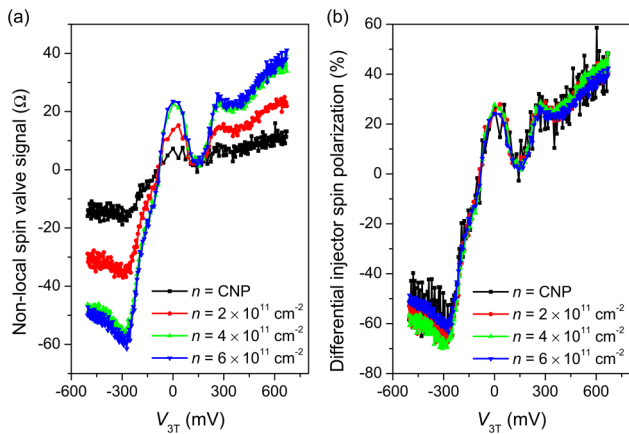

FIG. 3. (a) Measurement of the DC bias dependence of the R_{NL} at four different carrier concentrations, where Contact 1 is used as injector and Contact 5 as detector. (b) The extracted spin polarization of the injector contact using Eq. (1). The spin polarization reaches $p_{in} = -60\%$ at negative and $p_{in} = +40\%$ at positive I_{DC}. Measurements using Contact 2 as injector yield comparable results.
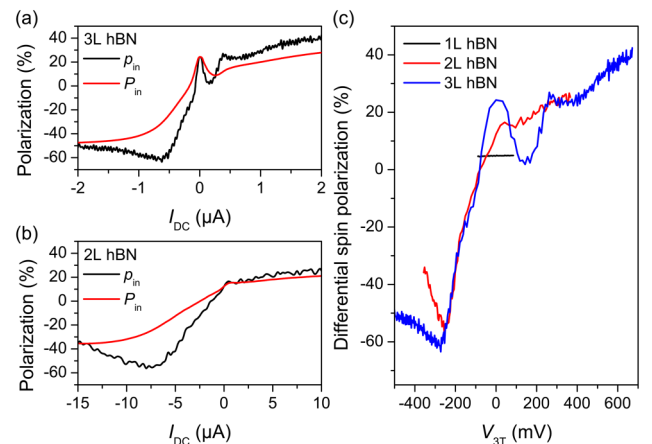

FIG. 4. Differential (p_{in}) and DC (P_{in}) injector spin polarization of (a) the 3L-hBN device using Contact 1 and Contact 5 and (b) the 2L-hBN device from Ref. 34. Note that the numerical integration of p_{in} averages the noise out of p_{in}. (c) Comparison of the differential spin polarizations of 1L-, 2L-, and 3L-hBN tunnel barriers. The data of 1L-hBN are taken from Ref. 21.

would be relevant, the measured Hanle curves would widen.[36] Consequently, the extracted spin lifetimes would decrease with increasing I_{DC}, which we do not observe here. Furthermore, our I_{DC} is at most $2\,\mu A$, whereas a sizable drift effect requires larger charge currents.[4] Local charge carrier drift at the injector, caused by pinholes in the barrier, was used to explain a modulation of the spin injection polarization.[14] From our measurements, we can exclude this mechanism as origin due to the negligible modulation of the spin injection polarization with n. Moreover, we use crystalline hBN as a tunnel barrier, which has the advantage over evaporated barriers that pinholes are not expected to be present.

V. CALCULATION OF THE DC SPIN POLARIZATION

For practical applications, a large DC spin polarization P is required. Using the differential spin polarization p, we can calculate P via[21]

$$p(I_{DC}) = \frac{dP(I_{DC})}{dI_{DC}} I_{DC} + P(I_{DC}), \qquad (2)$$

The results obtained for 3L- and 2L-hBN barriers using this procedure are shown in Figs. 4(a) and 4(b). The DC spin polarization of 3L-hBN rises close to 50%, whereas 2L-hBN yield only up to 35%. Measurements on vertical tunnel junctions with 1L- and 2L-hBN tunnel barriers reported a spin polarization of $\sim 1\%$ (1L) and 12% (2L).[35,37,38] This underlines the potential of cobalt/3L-hBN contacts for highly efficient spin injection into graphene.

The comparison of the differential spin polarization of 1L-, 2L-, and 3L-hBN/Co contacts is shown in Fig. 4(c). In the case of 1L-hBN, the polarization remains constant ($\sim 5\%$), mostly independent of the applied V_{3T} and clearly below the values of 2L- and 3L-hBN barriers. However, the comparison of 2L- and 3L-hBN yields comparable differential spin polarizations, whereas the electric fields underneath the contacts, which arise from V_{3T}, change from 1L- to 3L-hBN by a factor of 3. Therefore, local gating underneath the contacts can also be excluded as origin of the bias dependence. The effect of quantum capacitance is discussed in the supplementary material.

Zollner *et al.*[26] calculated the exchange coupling between cobalt and graphene separated by 1L- to 3L-hBN. Interestingly, they reported a spin splitting of up to 10 meV when cobalt and graphene are separated by 2L-hBN. For 3L-hBN, this splitting decreases to $18\,\mu eV$. Since we observe very comparable results between 3L-hBN and 2L-hBN, we conclude that proximity-induced exchange splitting is most likely not the origin for the DC bias dependent spin injection efficiency in Co/hBN/graphene.

VI. ISOTROPY OF THE SPIN INJECTION EFFICIENCY

By applying a large $B_\perp \sim 1.2\,T$, we can rotate the cobalt magnetization close to out-of-plane and characterize the spin injection efficiency of 3L-hBN tunnel barrier for out-of-plane spins. This measurement technique was used to determine the spin lifetime anisotropy of graphene,[39] which can also be measured using oblique spin precession with lower applied
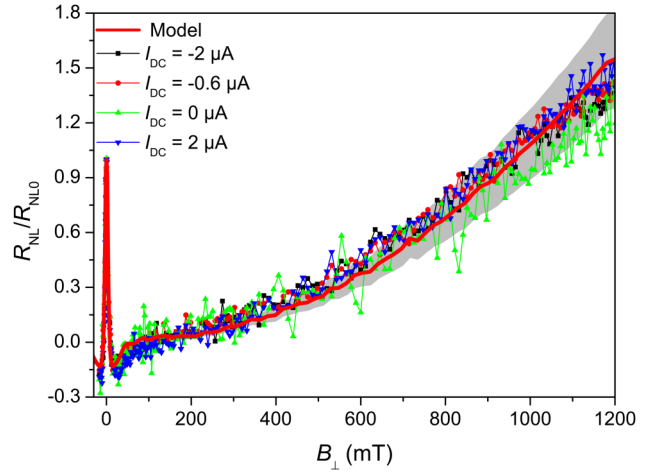

FIG. 5. Hanle spin precession curves measured up to $B_\perp = 1.2\,T$. For comparison, R_{NL} is normalized to R_{NL} at $B_\perp = 0$ (R_{NL0}). The measurements at different I_{DC} are shown as scattered lines, the red solid line is simulated with isotropic spin injection ($p_z/p_y = 1$).

magnetic fields.[29,40,41] By comparing both results, we can separate the anisotropy of the BLG channel from the anisotropy of the spin injection and detection polarization.

Figure 5 shows the Hanle curves measured at a carrier concentration of $n = 6 \times 10^{11}\,cm^{-2}$, which is the highest density accessible in our device and has been chosen to minimize the effect of magnetoresistance and the spin lifetime anisotropy of the BLG channel. The data are normalized to $R_{NL0} = R_{NL}(B_\perp = 0\,T)$, the gray shaded area is determined by the uncertainty of the extracted spin lifetime anisotropy. The normalized measurements at different I_{DC} overlap each other, which indicates that p_z/p_y is independent of I_{DC}.

We model the spin transport using the Bloch equations for anisotropic spin transport as discussed in Ref. 29. Additionally, we include the rotation of the contact magnetization, which we extract from anisotropic magnetoresistance measurements, shown in the supplementary material. The good agreement between the experimental data and our model suggests that the spin injection polarization is isotropic, and hence $p_z/p_y \approx 1$.

VII. TWO-TERMINAL DC SPIN TRANSPORT MEASUREMENTS UP TO ROOM TEMPERATURE

Lastly, we use the large DC spin polarization of our device to measure spin transport in a local two-terminal geometry, which is especially interesting for applications. For this experiment, we source a DC current (I_{DC}) and measure simultaneously the DC voltage V_{DC} between Contact 2 and Contact 1. The local, two-terminal signal is $R_{2T} = V_{DC}/I_{DC}$, with the spin signal $\Delta R_{2T} = \Delta R_{2T}(\uparrow\uparrow) - \Delta R_{2T}(\uparrow\downarrow)$ is $162\,\Omega$ at $I_{DC} = -2\,\mu A$ and $75\,\Omega$ at $I_{DC} = +1\,\mu A$.

A measurement of spin precession between Contact 3 and Contact 2 is shown in Fig. 6(c). We observe a clear Hanle curve and fit the data with $\tau_s = (740 \pm 60)\,ps$, $D_s = (560 \pm 70)\,cm^2/s$ and calculate $\lambda = 6.5\,\mu m$. Note that the change of these values compared to Table I was caused by an exposure of the sample to air. Using the spin
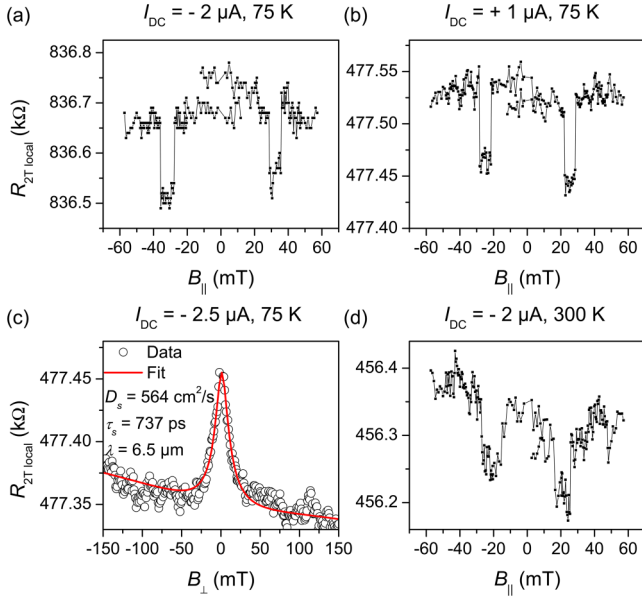
FIG. 6. (a) Two-terminal spin signal measured with $I_{DC} = -2\,\mu A$ and (b) $I_{DC} = +1\,\mu A$. (c) Hanle precession data measured at $T = 75\,K$ between Contact 3 and Contact 2 with $I_{DC} = -2.5\,\mu A$. (d) Room temperature spin valve measurement between Contact 2 and Contact 1 with $I_{DC} = -2\,\mu A$.

polarization of the biased contacts and the extracted spin relaxation length, we can calculate the expected local 2T spin valve signal[21]

$$\Delta R_{2T} = [P_A(+I_{DC})p_B(-I_{DC})$$
$$+ p_A(-I_{DC})P_B(+I_{DC})]\frac{R_{sq}\lambda}{w}e^{-d/\lambda}, \qquad (3)$$

where the indexes A and B denote both contacts at the bias I_{DC}. We calculate using the spin polarization values $\Delta R_{2T} = -177\,\Omega$ at $I_{DC} = -2\,\mu A$ and $R_{2T} = -108\,\Omega$ at $I_{DC} = +1\,\mu A$, which is in agreement with the measured data in Figs. 6(a) and 6(b) of $162\,\Omega$ and $80\,\Omega$.

The measurement of R_{2T} at room temperature is shown in Fig. 6(d). ΔR_{2T} is at room temperature $\sim 100\,\Omega$ and is clearly present, which indicates no dramatic change of the DC spin polarization with increasing temperature. These results underline the relevance of 3L-hBN barriers for graphene spintronics.

VIII. SUMMARY

In conclusion, we have shown that 3L-hBN tunnel barriers provide a large, tunable spin injection efficiency from cobalt into graphene. The zero bias spin injection polarization is between 20% and 30%, and the differential spin injection polarization can increase to -60% by applying a negative DC bias. The resulting DC spin polarization of up to 50% allows spin transport measurements in a DC two-terminal configuration up to room temperature. We study the n dependence of the spin injection polarization and find that it does not depend on n. From a comparison between 3L- and 2L-hBN, we observe that the DC bias dependence scales with the voltage and not the electric field, indicating that local gating is not the dominant mechanism. We also

compare the spin injection polarization for in-plane and out-of-plane spins and find that it is isotropic and that p_z/p_y is independent of the applied DC bias.

During the preparation of this manuscript, we became aware of a related work,[42] where also a DC bias dependent spin signal is reported in Co/SrO/graphene heterostructures. Furthermore, the authors also exclude carrier drift as origin.

Supplementary Material

See supplementary material for details on the determination of the unbiased spin polarization, the asymmetry and temperature-dependence of the IV characteristics, the determination of the magnetization angle, the quantum capacitance correction, and the full set of spin transport measurements.

[1]D. Huertas-Hernando, F. Guinea, and A. Brataas, Phys. Rev. B **74**, 155426 (2006).

[2]W. Han, R. K. Kawakami, M. Gmitra, and J. Fabian, Nat. Nanotechnol. **9**, 794 (2014).

[3]S. Roche, J. Åkerman, B. Beschoten, J.-C. Charlier, M. Chshiev, S. P. Dash, B. Dlubak, J. Fabian, A. Fert, M. H. D. Guimarães, F. Guinea, I. Grigorieva, C. Schönenberger, P. Seneor, C. Stampfer, S. O. Valenzuela, X. Waintal, and B. J. van Wees, 2D Mater. **2**, 030202 (2015).

[4]J. Ingla-Aynés, R. J. Meijerink, and B. J. van Wees, Nano. Lett. **16**, 4825 (2016).

[5]M. Drögeler, C. Franzen, F. Volmer, T. Pohlmann, L. Banszerus, M. Wolter, K. Watanabe, T. Taniguchi, C. Stampfer, and B. Beschoten, Nano. Lett. **16**, 3533 (2016).

[6]P. J. Zomer, M. H. D. Guimarães, N. Tombros, and B. J. van Wees, Phys. Rev. B **86**, 161416 (2012).

[7]M. H. D. Guimarães, P. J. Zomer, J. Ingla-Aynés, J. C. Brant, N. Tombros, and B. J. van Wees, Phys. Rev. Lett. **113**, 086602 (2014).

[8]M. Drögeler, F. Volmer, M. Wolter, B. Terrés, K. Watanabe, T. Taniguchi, G. Güntherodt, C. Stampfer, and B. Beschoten, Nano. Lett. **14**, 6050 (2014).

[9]J. Ingla-Aynés, M. H. D. Guimarães, R. J. Meijerink, P. J. Zomer, and B. J. van Wees, Phys. Rev. B **92**, 201410 (2015).

[10]M. Gurram, S. Omar, S. Zihlmann, P. Makk, C. Schönenberger, and B. J. van Wees, Phys. Rev. B **93**, 115441 (2016).

[11]S. Singh, J. Katoch, J. Xu, C. Tan, T. Zhu, W. Amamou, J. Hone, and R. K. Kawakami, Appl. Phys. Lett. **109**, 122411 (2016).

[12]G. Schmidt, L. W. Molenkamp, A. T. Filip, and B. J. van Wees, Phys. Rev. B **62**, R4790 (2000).

[13]E. I. Rashba, Phys. Rev. B **62**, R16267 (2000).

[14]C. Józsa, M. Popinciuc, N. Tombros, H. T. Jonkman, and B. J. van Wees, Phys. Rev. B **79**, 081402 (2009).

[15]W. Han, K. Pi, K. M. McCreary, Y. Li, J. J. I. Wong, A. G. Swartz, and R. K. Kawakami, Phys. Rev. Lett. **105**, 167202 (2010).

[16]F. Volmer, M. Drögeler, E. Maynicke, N. Von Den Driesch, M. L. Boschen, G. Güntherodt, and B. Beschoten, Phys. Rev. B **88**, 161405 (2013).

[17]F. Volmer, M. Drögeler, E. Maynicke, N. Von Den Driesch, M. L. Boschen, G. Güntherodt, C. Stampfer, and B. Beschoten, Phys. Rev. B **90**, 165403 (2014).

[18]T. Yamaguchi, Y. Inoue, S. Masubuchi, S. Morikawa, M. Onuki, K. Watanabe, T. Taniguchi, R. Moriya, and T. Machida, App. Phys. Express **6**, 073001 (2013).

[19]M. V. Kamalakar, A. Dankert, J. Bergsten, T. Ive, and S. P. Dash, Sci. Rep. **4**, 6146 (2015).

[20]M. V. Kamalakar, A. Dankert, P. J. Kelly, and S. P. Dash, Sci. Rep. **6**, 21168 (2016).

[21]M. Gurram, S. Omar, and B. van Wees, Nat. Commun. **8**, 248 (2017).

[22]A. Avsar, J. Y. Tan, M. Kurpas, M. Gmitra, K. Watanabe, T. Taniguchi, J. Fabian, and B. Özyilmaz, Nat. Phys. **13**, 888 (2017).

[23]I. Neumann, M. V. Costache, G. Bridoux, J. F. Sierra, and S. O. Valenzuela, Appl. Phys. Lett. **103**, 112401 (2013).

[24]S. Singh, J. Katoch, T. Zhu, R. J. Wu, A. S. Ahmed, W. Amamou, D. Wang, K. A. Mkhoyan, and R. K. Kawakami, Nano. Lett. **17**, 7578 (2017).

[25]M. Gurram, S. Omar, and B. J. van Wees, 2D Mater. **5**, 032004 (2018).

[26]K. Zollner, M. Gmitra, T. Frank, and J. Fabian, Phys. Rev. B **94**, 155441 (2016).

[27]S. Ringer, M. Rosenauer, T. Völkl, M. Kadur, F. Hopperdietzel, D. Weiss, and J. Eroms, Appl. Phys. Lett. **113**, 132403 (2018).

[28]P. J. Zomer, M. H. D. Guimarães, J. C. Brant, N. Tombros, and B. J. van Wees, Appl. Phys. Lett. **105**, 013101 (2014).

[29]J. C. Leutenantsmeyer, J. Ingla-Aynés, J. Fabian, and B. J. van Wees, Phys. Rev. Lett. **121**, 127702 (2018).

[30]F. J. Jedema, A. T. Filip, and B. J. van Wees, Nature **410**, 345 (2001).

[31]F. J. Jedema, H. B. Heersche, A. T. Filip, J. J. A. Baselmans, and B. J. van Wees, Nature **416**, 713 (2002).

[32]N. Tombros, C. Jozsa, M. Popinciuc, H. T. Jonkman, and B. J. van Wees, Nature **448**, 571 (2007).

[33]T. Maassen, I. J. Vera-Marun, M. H. D. Guimaräes, and B. J. van Wees, Phys. Rev. B **86**, 235408 (2012).

[34]J. C. Leutenantsmeyer, T. Liu, M. Gurram, A. A. Kaverzin, and B. J. van Wees, Phys. Rev. B **98**, 125422 (2018).

[35]M. Piquemal-Banci, R. Galceran, F. Godel, S. Caneva, M.-B. Martin, R. S. Weatherup, P. R. Kidambi, K. Bouzehouane, S. Xavier, A. Anane, F. Petroff, A. Fert, S. Mutien-Marie Dubois, J.-C. Charlier, J. Robertson, S. Hofmann, B. Dlubak, and P. Seneor, ACS. Nano **12**, 4712 (2018).

[36]B. Huang and I. Appelbaum, Phys. Rev. B **77**, 1 (2008).

[37]A. Dankert, M. Venkata Kamalakar, A. Wajid, R. S. Patel, and S. P. Dash, Nano. Res. **8**, 1357 (2015).

[38]P. U. Asshoff, J. L. Sambricio, A. P. Rooney, S. Slizovskiy, A. Mishchenko, A. M. Rakowski, E. W. Hill, A. K. Geim, S. J. Haigh, V. I. Fal'Ko, I. J. Vera-Marun, and I. V. Grigorieva, 2D Mater. **4**, 031004 (2017).

[39]N. Tombros, S. Tanabe, A. Veligura, C. Jozsa, M. Popinciuc, H. T. Jonkman, and B. J. van Wees, Phys. Rev. Lett. **101**, 046601 (2008).

[40]B. Raes, J. E. Scheerder, M. V. Costache, F. Bonell, J. F. Sierra, J. Cuppens, J. van de Vondel, and S. O. Valenzuela, Nat. Commun. **7**, 11444 (2016).

[41]B. Raes, A. W. Cummings, F. Bonell, M. V. Costache, J. F. Sierra, S. Roche, and S. O. Valenzuela, Phys. Rev. B **95**, 085403 (2017).

[42]T. Zhu, S. Singh, J. Katoch, H. Wen, K. Belashchenko, I. Žutic, and R. K. Kawakami, Phys. Rev. B **98**, 054412 (2018).